Ion Dynamics at the Carbon Electrode/Electrolyte Interface: Influence of Carbon Nanotubes Types

Freddy Escobar-Teran, Hubert Perrot, Ozlem Sel

Ion dynamics at the carbon electrode/electrolyte interface: Influence of carbon nanotubes types

Freddy Escobar-Teran[1,2], Hubert Perrot* [1] and Ozlem Sel [1]

[1] Laboratoire Interfaces et Systèmes Electrochimiques, LISE, UMR8235, Sorbonne Université, CNRS, F-75005 Paris, France; fescobarteran@hotmail.com (F.E.-T.); hubert.perrot@sorbonne-universite.fr (H.P.)
[2] Departamento de Ciencias Exactas, Universidad de las Fuerzas Armadas-ESPE, 171103 Sangolqui, Ecuador
* Correspondence: hubert.perrot@sorbonne-universite.fr

Abstract: Electrochemical quartz crystal microbalance (EQCM) and ac-electrogravimetry methods were employed to study ion dynamics in carbon nanotube base electrodes in NaCl aqueous electrolyte. Two types of carbon nanotubes, Double Wall Carbon Nanotube (DWCNT) and Multi Wall Carbon Nanotube (MWCNT) were chosen due to their variable morphology of pores and structure properties. The effect of pore morphology/structure on the capacitive charge storage mechanisms demonstrated that DWCNT base electrodes are the best candidates for energy storage applications in terms of current variation and specific surface area. Furthermore, the mass change obtained via EQCM showed that DWCNT films is 1.5 times greater than MWCNT films at the same potential range. In this way, the permselectivity of DWCNT films showed cation exchange preference at cathode potentials while MWCNT films showed anion exchange preference at anode potentials. The relative concentration obtained from ac-electrogravimetry confirm that DWCNT base electrodes are the best candidates for charge storage capacity electrodes, since they can accommodate higher concentration of charged species than MWCNT base electrodes.

Keywords: carbon nanotubes; DWCNT, MWCNT; electrochemical quartz crystal microbalance; EQCM; electrode/electrolyte interface; ion transfer.

1. Introduction

The development of energy storage systems (supercapacitors/batteries) to decrease the energy consumption coming from fossil fuels is a way towards a more environmentally friendly society. However, the efficiency of these electrochemical devices depends on the elements constituting them such as the electrode material, which plays an important role to achieve better supercapacitor performances [1, 2].

In supercapacitors, the charge storage is based on a reversible adsorption of electrolyte ions towards the surface of electrodes [3-8]. Therefore, the selection of the electrode materials is important due to a certain number of parameters such as: specific surface area, porosity, structure, electrical conductivity, surface wettability, and electrochemical stability to improve the performance of electrodes [2, 9-12]. In this way, carbon nanotubes have been used for supercapacitors due to their novel properties such as high electrical conductivity, high charge transport capability, unique pore structure and high specific surface area where the charges are continuously distributed [13, 14].

However, the ion dynamics studies at the interfaces are experimentally difficult because there are not many appropriate electrochemical or physico-chemical methods that provide direct access to this kind of information.

Electrochemical quartz crystal microbalance (EQCM) has been extensively used to investigate the charge storage mechanisms in porous materials. EQCM is a powerful in situ technique to measure ionic fluxes at the electrode interfaces, which current responses (ΔI) and global gravimetric changes (Δm) at the electrode/electrolyte interface are monitored during the electrochemical process. Over the past decade, Levi, M. D., et al. have

widely employed EQCM to study the charge-compensation mechanism in carbon micropores and particularly, the effect of specific adsorption of ions with different sizes [15-20]. Continuing these achievements, EQCM was also used to investigate the charge compensation mechanism between electrode/electrolyte interface [21]and the hydration/solvation effect on the capacitive performance [22, 23]. Recently, EQCM has been employed to study the electrolyte concentration effect on the capacitive behavior as well as the compositional changes in porous films [24]. Finally, EQCM combined with nuclear magnetic resonance (NMR) has been employed to understand in a deep manner the charge mechanism in the electrical double layer [25].

Another interesting aspect of the EQCM, is the capability to estimate mass and charge variations simultaneously which provides to access to the derivation of the global mass per mole of electrons (MPE) exchanged at the electrochemical interface. By this way the MPE corresponds to its molar mass when one specie is exchanged but if multiple ion transfer occurs, EQCM remains limited to interpret the contribution of different species [22, 24]. In order to identify the contribution of different species EQCM equations were developed incorporating Donnan type electrical double layer models [26]. Furthermore, EQCM with dissipation monitoring (EQCM-D) can be used to study the viscoelastic properties e.g. formation of a solid electrolyte interface (SEI) layer as well as the complex mass changes of the electrodes [27-30]. This acoustic technique permits to identify the effect of several parameters such as the nature of the electrolytes/ions or the binder on the structure change of the electrodes [31].

Here, an alternative electrochemical and gravimetric method called ac-electrogravimetry was used to complement the EQCM based methods in the energy storage domain. Ac-electrogravimetric methodology has been used to study the charge compensation mechanisms in carbon nanotubes, [32, 33] reduced graphene oxide [34, 35], pseudocapacitive metal oxide-based electrodes [25, 36] and nanocomposite electrodes [34, 37]. Recently, it has been employed to investigate the ion insertion mechanisms in aqueous proton-based batteries [38]. Ac-electrogravimetry is a multi-scale coupled electrogravimetric method (quartz crystal microbalance and electrochemical impedance) through which it provides relevant information concerning: (i) identification and kinetic of electroadsorption/desorption of species at the electrode/electrolyte interface, (ii) separation of the charged and non-charged species involved at the electrode/electrolyte interface , and (iii) the relative concentration variations of the species within the material. Therefore, the ac-electrogravimetric methodology was proposed here to study/compare the capacitive behavior in different types of carbon nanotube electrodes.

2. Materials and Methods

2.1. Materials

Double Wall CNT (755141-1G, length: 3 μm and diameter: 3.5 nm) and Multi Wall CNT (75517-1G, length: 1 μm and diameter: 9.5) were acquired at Sigma Aldrich Company.

2.2. *CNT Thin Films Electrode Preparation*

CNT films were prepared according to the method described in previous papers [32, 34, 39]. A solution containing 90% carbon (9 mg) CNT powder and 10% (1 mg) poly(vinylidene fluoride-hexafluoropropylene) (PVDF-HFP) polymer binder in 10 mL of N-methyl-2-pyrrolidone was prepared to elaborate CNT films. Around 8μL of this solution was deposited through "drop-casting "method on a gold electrode which has an effective surface area of 0.20 cm^2 and keeps connected to a quartz crystal resonator (9 MHz-AWS, Valencia, Spain). After that, the carbon films followed a heat treatment with a heating rating of ~5°C min^{-1} until 120°C for 30 min. This treatment was necessary to eliminate the residual solvent and improve the linkage of films on QCM electrode. The deposited mass was cal-

culated by using the Sauerbrey equation, $\Delta f_m = -k_s \Delta m$ where Δf_m is the microbalance frequency change, k_s is the experimental calibration constant ($16.3 \times 10^{+7}$ Hz/g·cm^{-2}) and Δm corresponds to the mass change. It was got by measuring Δf_m, microbalance frequency change before and after deposition.

2.3. Morphological and Physical Characterizations

The CNT powders were characterized by Brunauer-Emmett-Teller methods (BET), X-ray diffraction (XRD), and high-resolution transmission electron microscopy (HR-TEM). Details about the characteristics and selected parameters of these equipment are described in a previous paper [33].

Field emission gun scanning electron microscopy (FEG-SEM) (Zeiss, Supra 55) was also employed to investigate the surface morphology of the CNT films. In our experiments, FEG-SEM (Field Emission Gun – Scanning Electron Microscope) provides a very highest resolution imaging compared to regular SEM. The samples were previously prepared onto an aluminum stub with a conductive carbon tape and sputter-coated with gold (JEOL JFC-1300 Auto fine coater).

2.4. EQCM and ac-electrogravimetric characterization

EQCM measurements were carried out in NaCl aqueous solutions and using a three-electrode configuration. A lab-made QCM device (Miller oscillator) was employed to measure frequency shift (Δf) of the quartz crystal resonators. A gold electrode of the quartz resonator was used as the working electrode. Platinum grid and Ag/AgCl (3M KCl) was used as counter and reference electrode, respectively (See Figure 1). The gravimetric regime was assured by keeping film thickness acoustically thin (< 200 nm).

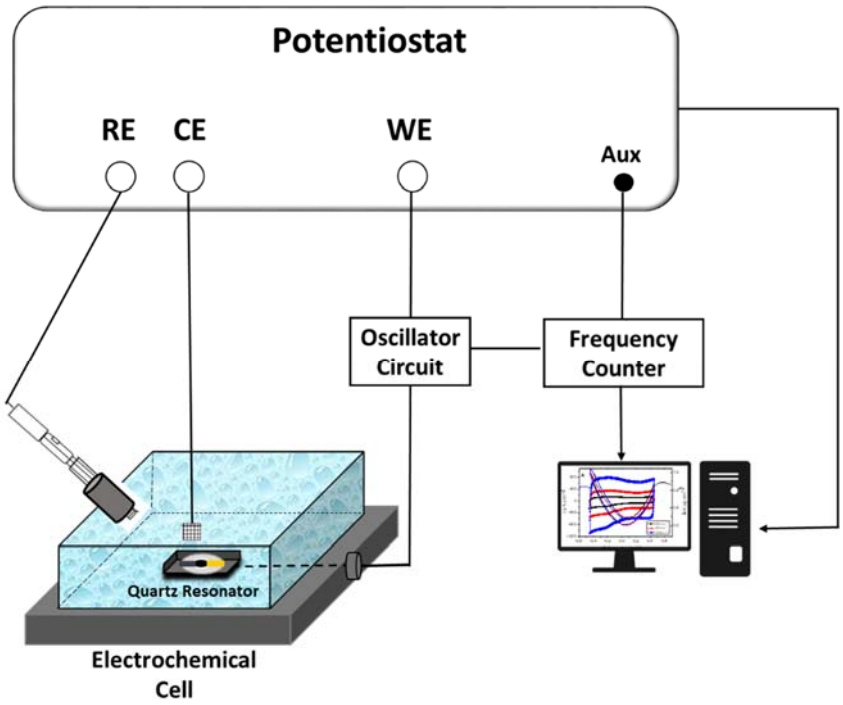

Figure 1. Experimental set-up of an EQCM

A QCM set-up connected to a four-channel frequency response analyzer (FRA, Solartron 1254) and a lab-made potentiostat (SOLETEM-PGSTAT) were employed to get ac-

electrogravimetric measurements. The QCM measurements were carried out under dynamic regime, following the potential modulation operating at various frequencies, the electrochemical system being polarized at selected potentials.

In order to get a dynamic regime a sinusoidal small amplitude potential perturbation was superimposed. The frequency intervals were since 63 KHz until 10 mHz. The ac response, ΔI, of the electrochemical system and the mass change, Δm, of the working electrode were simultaneously measured, which resulted in the electrogravimetric TF, $(\Delta m/\Delta E(\omega))$ and the electrical TF $(\Delta E/\Delta I(\omega))$. These transfer functions were obtained simultaneously at a given potential and frequency modulation, f (pulsation, $\omega = 2\pi f$). The working principle and ac-electrogravimetric measurement setup have been detailed previously [34, 36, 40, 41].

3. Results and Discussion

3.1. Material characteristics

DWCNTs and MWCNTs constituting the composite electrodes were characterized by HRTEM. The images in Figures 2A and C indicate that the diameter of the DWCNTs and MWCNTs is between: about ~ 4 nm and ~8 nm respectively. Nitrogen sorption measurements and XRD were used to characterize the specific surface area and crystallinity of the CNTs. The Brunauer–Emmett–Teller (BET) specific surface area of the DWCNTs and MWCNTs were estimated to be 552 $m^2 \cdot g^{-1}$ and 300 $m^2.g^{-1}$ respectively and the crystallinity attributed to the hexagonal graphitic structure [42] were observed on (002) and (001) reflections (See Figures SI.1 and SI.2). Then, the CNT electrodes were deposited on the gold patterned quartz resonators. For that, the PVDF-HFP was used as a binder polymer to adherer the CNT on the gold quartz resonator. Figures 2B and D show a FEG-SEM image of the DWCNT and MWCNT film electrodes, which reveal a high-density of CNTs bundles.

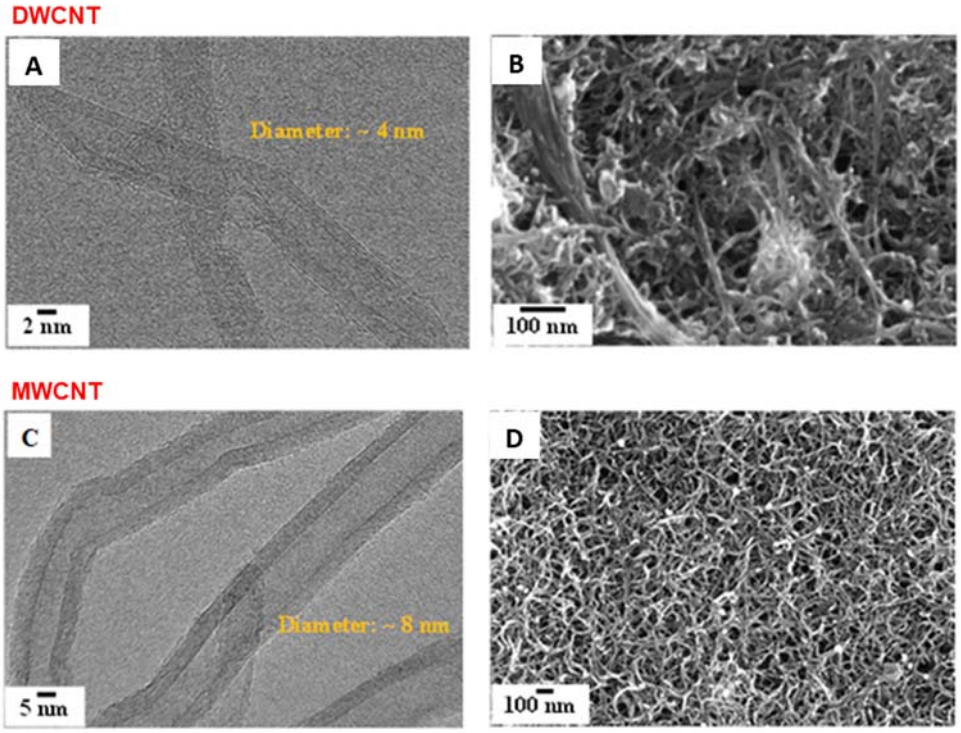

Figure 2. HRTEM images of the DWCNTs (A) MWCNTs (C) and FEG-SEM images of, DWCNT (B), MWCNT (D) based thin films deposited on the gold patterned quartz resonator.

3.2. EQCM study of CNTs in 0.5 M NaCl

The EQCM results of CNT thin films obtained in aqueous electrolytes of 0.5 M NaCl are shown in Figure 3. A growing capacitive current is observed when the scan rate increases (Figure 3A and B) for all the films. Besides, DWCNT films show a higher capacitive current than MWCNT films and even more than SWCNT described in previous paper [32]. This difference in current is probably due to the pore structure of the materials and its accessibility to the electrolyte ions which is contradictory with the specific surface area determined on the CNT powder but not with the CNTs films. In this study, DWCNT and MWCNT films show quasi-rectangular shaped responses indicating that the charge storage capacity is mainly due to the reversible adsorption/desorption of electrolyte ions. The slight distortion from a perfect rectangular shape is attributed to the presence of a slight faradaic contribution to the charge storage as already mentioned [32, 33].

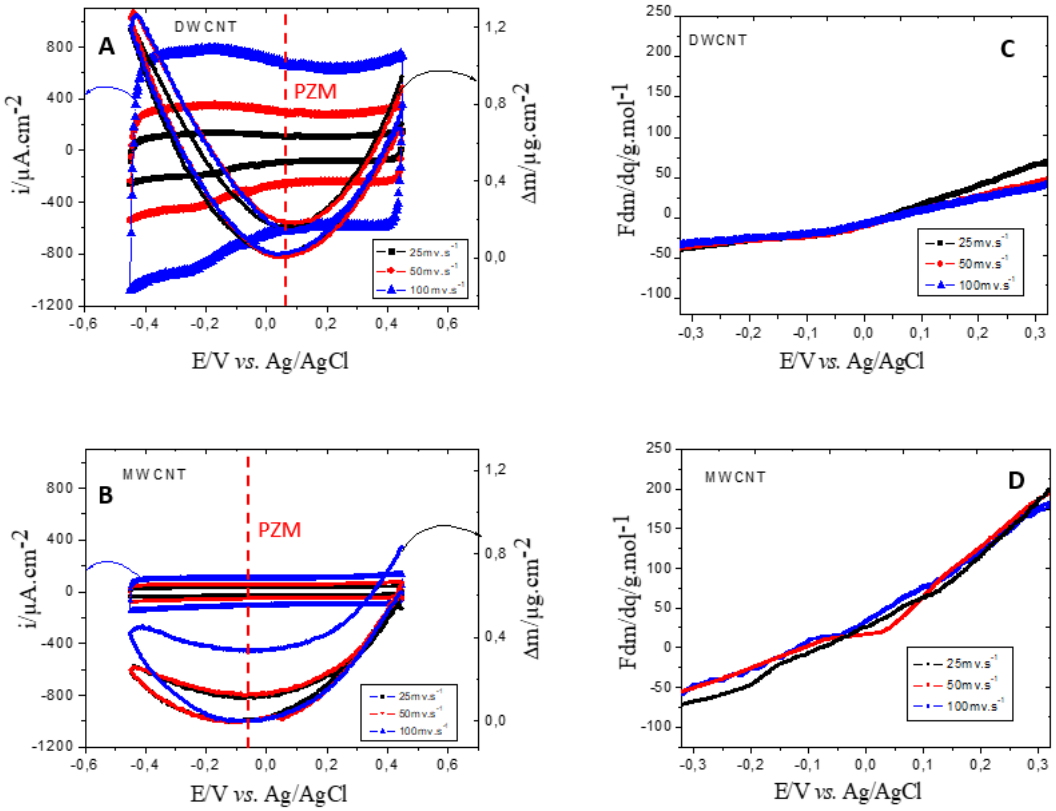

Figure 3. EQCM results of DWCNT (A), and MWCNT (B) measured in 0.5 M NaCl aqueous electrolyte. The average molecular weight values of the species involved in the electrochemical process showed as a function of the potential obtained from the reduction branch of EQCM data are presented in panels C–D.

Regarding the mass changes, the DWCNT and MWCNT follow the same order as the current values, i.e., $\Delta m_{DWCNT} > \Delta m_{MWCNT}$. Also, the reversibility of the mass response is better appreciated in DWCNT than in MWCNT (Figure 3A and B) where a large hysteresis was observed in MWCNT. For the DWCNT, the mass change is higher at cathodic potentials than at anodic potentials while in MWCNT, the mass change is slightly more significant at anodic potentials than at cathodic potentials. It is also observed that the PZC is shifted slightly towards more cathodic potentials (Figure 3B). The PZC or PZM is the point where the charge/masse is equal to zero and these corresponds to the potentials of 0.075±0.25 V for DWCNT and -0.075±0.25 V for MWCNT follow the following order: $PZM_{DWCNT} < PZM_{MWCNT}$. In other words, DWCNT films show cations exchange preference while

MWCNT films show anions exchange preference at same potential range. Also, the V-shape observed in the mass changes (Figure 3A and B) is due to the selective adsorption/desorption of cationic and anionic species in the potential range [32, 43].

The average molecular weight values, $\frac{Fdm}{dq}\left(=F\frac{dm}{dt}x\frac{1}{i}\right)$, of the species involved in the electrochemical process showed as a function of the potential are obtained from the reduction branch of EQCM data presented in Figure 3A and B.

Figure 3C and D show the average molecular weight values of the electroadsorbed species if only one ion is transferred. The values are calculated as a function of the applied potential in the NaCl electrolyte. The values vary in the range of 50 to -35 g.mol^{-1} and 180 to -70 g.mol^{-1}, for the DWCNT and MWCNT thin films, respectively. From the two Figures 3C and D, it should be noted that for anodic potentials, positive Fdm/dq values are estimated which corresponds to anion contribution. As for cathodic potentials, negative Fdm/dq values were calculated indicating the cation contribution. In all the cases, higher or lower atomic weight compared to Na^+ or Cl^- ions are found which indicates a complex ion transfer behavior associated with solvent contribution. The observed higher values further indicate that the ions are hydrated and/or accompanied by free solvent molecules during their transfer in the same direction. Particularly in MWCNT, higher values at anodic potentials are observed which could correspond to anions accompanied by free solvent molecules.

3.3. Ac-electrogravimetric study of CNT thin film electrodes in 0.5 M NaCl.

Analysis of ac-electrogravimetric responses of DWCNT and MWCNT film electrodes are presented in Figure 4 in a comparative manner at a selected potential (-0.4V) in the cathodic part.

First, the charge/potential transfer functions (TFs), $\frac{\Delta q}{\Delta E}(\omega)$, permit a suitable separation of the ionic contributions, however, without any possibility to identify the ionic species involved.

In figures 4A and C for DWCNT and MWCNT films respectively a one big loop is observed which can be assigned to only one specie. However, two species can be also assigned regarding that the time constants of ions are not really different from each other.

To clarify these ideas, the mass /potential transfer functions, $\frac{\Delta m}{\Delta E}(\omega)$, is used. Figures 4B and D show a big loop in the third quadrant from 100 to 1 Hz which is characteristic of cation and free solvent molecules in the same flux directions, as described previously[40, 41].

The experimental TFs in Figure 4 were fitted using the Equations A2-A3 (Appendix A): firstly, the number of species intervening and their respective K_i and G_i parameters were estimated from $\frac{\Delta E}{\Delta I}(\omega)$ or $\frac{\Delta q}{\Delta E}(\omega)$. These two key parameters were also used for the fitting of the experimental $\frac{\Delta m}{\Delta E}(\omega)$ TF. Then, identification of the involved species was achieved by fitting the experimental data with the theoretical $\frac{\Delta m}{\Delta E}(\omega)$ TF which is shown in equation A4 where the molar masses of the species (M_i) intervene in this equation. Here, for two films, the molar masse represents H^+ (c1) and $Na^+.H_2O$ (c2) for cations and free solvent (s) molecules in the same flux direction (Figure4). Furthermore, at selected potential (-0.4V), there is no anion contributions which is coherent in this potential region [32, 33].

The presence of two different cationic species and the free solvent molecules contribution estimated by simulating the experimental data was further confirmed by a fair analysis of the partial electrogravimetric transfer functions, for example, by removing the c2 contribution and calculating $\left.\frac{\Delta q}{\Delta E}\right|_{th}^{c1s}(\omega)$, by removing the c1 contribution and calculating $\left.\frac{\Delta q}{\Delta E}\right|_{th}^{c2s}(\omega)$, (Equations (A5) and (A6), no anion contribution at -0.4 V). The fitting results concerning the partial electrogravimetric transfer functions are given in Figure SI.3. A good fit also appears for the partial TFs including the same group of parameters, reinforcing the hypothesis of the different ion contributions (Table 1).

Table 1. K_i (kinetics of transfer), and G_i (inverse of the transfer resistance), Rt_i (transfer resistance) values extracted from the fitting results from ac-electrogravimetric measurements in aqueous 0.5 M NaCl at -0.4 V vs. Ag/AgCl for DWCNT and MWCNT films.

	M_i ($g.mol^{-1}$)	Species identification	K_i ($cm.s^{-1}$)	G_i ($mol.\ s^{-1}.cm^{-2}.V^{-1}$)	$Rt_i = 1/FG_i$ $ohm.cm^2$
DWCNT					
c2	23 + 18	$Na^+.H_2O$	$2.89x10^{-3}$	4.65×10^{-6}	2.22
s	18	H_2O	6.28×10^{-4}	9.11×10^{-7}	11.37
c1	1	H^+	3.64×10^{-5}	1.39×10^{-8}	745.52
MWCNT					
c2	23 + 18	$Na^+.H_2O$	5.66×10^{-3}	1.10×10^{-6}	9.42
s	18	H_2O	5.03×10^{-4}	5.23×10^{-6}	1.98
c1	1	H^+	2.39×10^{-4}	3.58×10^{-9}	2894.61

In addition, the species contribution was seen previously using electrochemical modulation showing different kinetics of transfer [44] e.g. Hillman et al. monitored the kinetic of species in nickel hydroxide thin films by combining EQCM and probe beam deflection (PBD) [45-47].

Figure 4 shows the ac-electrogravimetric results at - 0.4V vs. Ag/AgCl. In fact, it was measured from -0.45 V to 0.45 V vs. Ag/AgCl to have a complete electrochemical exploration of our system. The nature of the species (M_i) and the corresponding K_i and G_i constants were estimated as a function of potential [34, 36, 48].

Figure 5 shows the variation of the constant transfer kinetics, K_i, of the species as a function of the applied potential. Based on the K_i values presented in Figure 5A and B, the $Na^+.H_2O$ and Cl^- ions are the fastest of all species for SWCNT and MWCNT films. Here, the number of water molecule associated to the sodium ions is found to be n=1 for all the potentials. Furthermore, the transfer kinetics of free water molecules are somewhat close to the values of the chlorine ions at anode potentials. In addition, these water molecules accompany the transfer of $Na^+.H_2O$ and Cl^-, most likely due to an electrodragging phenomena [32, 33].

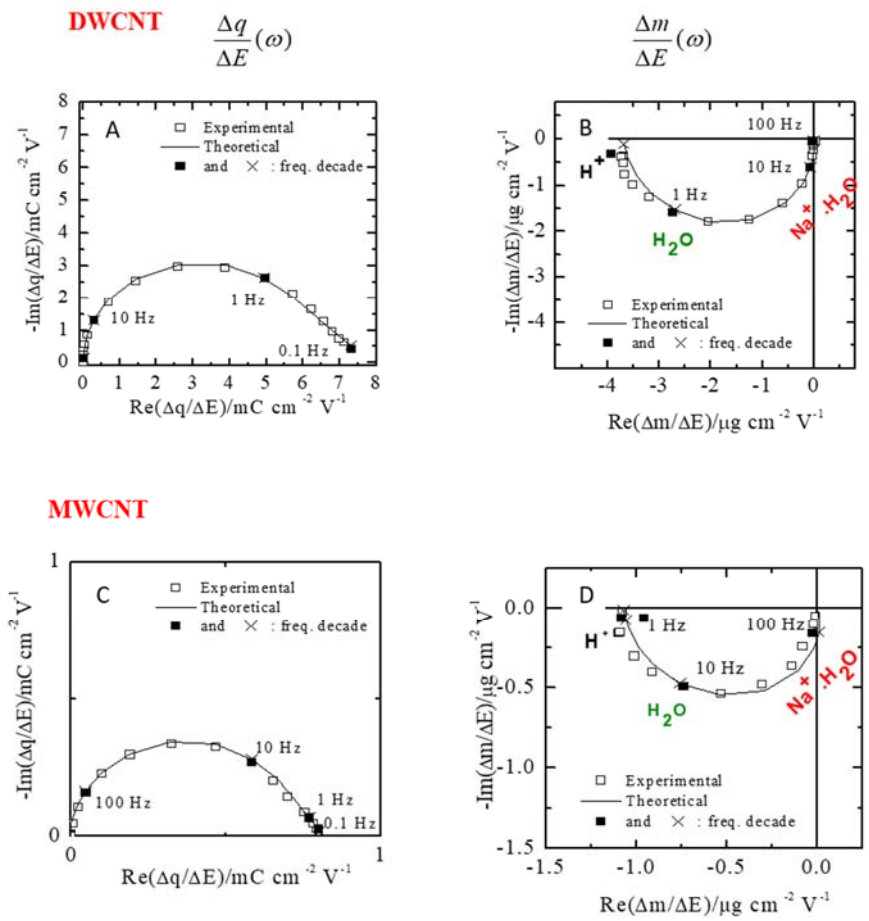

Figure 4. Experimental and theoretical ac-electrogravimetric data of the CNT thin films in 0.5 M NaCl measured at - 0.4V vs. Ag/AgCl. (A and C) $\frac{\Delta q}{\Delta E}(\omega)$, (B and F) $\frac{\Delta m}{\Delta E}(\omega)$. The parameter values of K_i, G_i and Rt_i are shown in Table 1.

Finally, the H^+ ion is the slowest species at cathodic potentials for DWCNT and MWCNT films (Figures 5A and B) showing similar order of magnitude of K_i values which is coherent with their substantially lower concentration in the media.

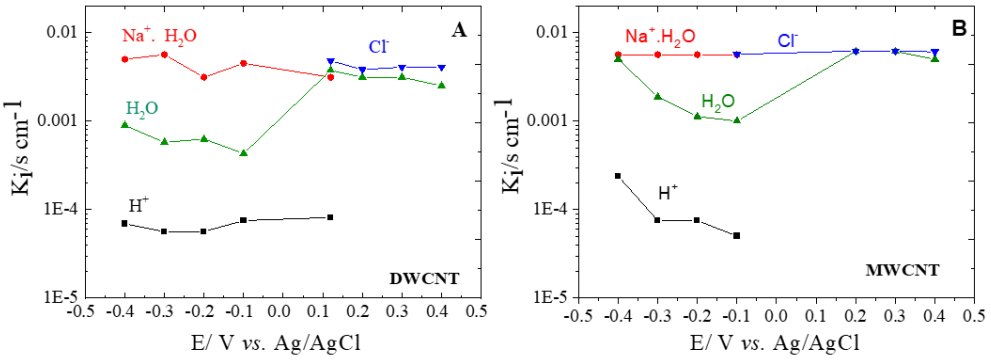

Figure 5. Kinetic constants of interfacial transfer, K_i, DWCNT (A), MWCNT (B) estimated from the fitting of the ac-electrogravimetric data and measured in aqueous 0.5M NaCl.

In order to quantify the role of each species, $\left.\frac{\Delta C_i}{\Delta E}\right|_{\omega\to 0} = -\frac{G_i}{K_i}$ has been calculated as a function of the applied potential using the parameters given by the ac-electrogravimetric fitting. Figure 6 shows the integration of $\left.\frac{\Delta C_i}{\Delta E}\right|_{\omega\to 0}$ against potential gives the relative concentration change, $(C_i\text{-}C_0)$ of the charged and non-charged species. For MWCNTs (Figure 6B), the $(C_i\text{-}C_0)$ values of the H_2O are higher than the $(C_i\text{-}C_0)$ values of the $Na^+.H_2O$, Cl^- and H^+.

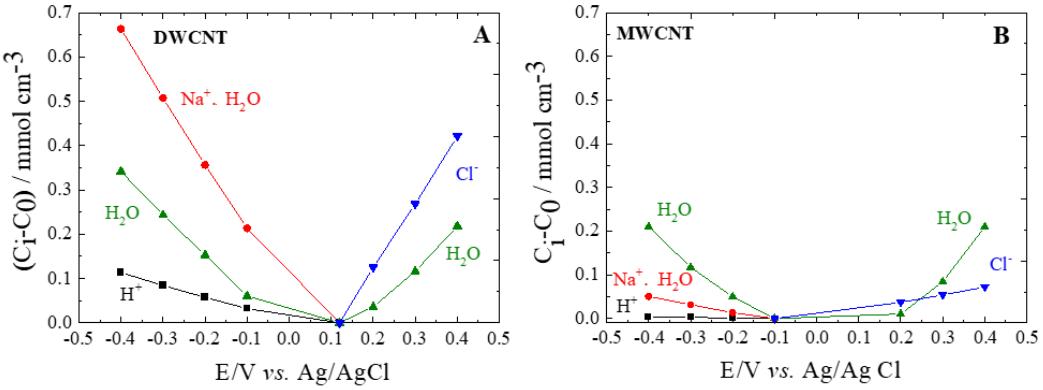

Figure 6. Evolution of the relative concentration, $C_i\text{-}C_0$, for DWCNT (A), MWCNT (B) of the charged and non-charged species over the applied potential and measured in aqueous 0.5M NaCl.

In contrast to MWCNT, in DWCNTs, the evolution of relative concentration of species presents a different trend. In comparison with the other species, the $(C_i\text{-}C_0)$ values of the $Na^+.H_2O$ are higher than the $(C_i\text{-}C_0)$ values of H^+ and H_2O at cathode potentials (Figures 6A). In conclusion, these results indicate that DWCNTs appear to be the best candidate for charge storage capacity electrodes, since it can accommodate higher concentration of charged species in DWCNTS than in MWCNTs.

4. Conclusions

Carbon nanotubes (CNTs) of "double-walled" (DWCNT), and "multi-walled" (MWCNT) films were elaborated on gold electrodes of microbalance and tested in NaCl aqueous electrolyte. The effect of pore morphology/structure but also roughness or hydrophilicity over the classical electrochemical responses demonstrated that DWCNT are better candidates for energy storage applications than MWCNT base electrodes in terms of current/mass variation and permselectivity of cations. The mass change obtained via EQCM showed that DWCNT films is 1.5 times greater than MWCNT films at the same range of potential. In this way, the permselectivity of DWCNT films showed cation exchange preference at cathode potentials while MWCNT films showed anion exchange preference at anode potentials. The relative concentration obtained from ac-electrogravimetry confirm that DWCNT base electrodes are the best candidates for polarizable electrodes, since they can accommodate higher concentration of charged species than MWCNT and even more than SWCNT base electrodes described in previous paper [32].

Appendix A

For different types of CNT films, the concentration transfer function, $\left.\frac{\Delta C_i}{\Delta E}\right|_{th}(\omega)$, of cation1 (*c1*), cation 2 (*c2*), anion (*a*) and free solvent (*s*)) were calculated through:

$$\left.\frac{\Delta C_i}{\Delta E}\right|_{th}(\omega) = \frac{-G_i}{j\omega d_f + K_i} \quad \text{(A1)}$$

where $\omega = 2\pi f$ is the pulsation, d_f is the film thickness , K_i represents the kinetics transfer, whereas G_i describes the ease/difficulty of ionic species (*c1* and *c2*) to be transferred at the electrode/electrolyte interface. Also, the transfer resistance, Rt_i, can determined through G_i using the following expression: $Rt_i = 1/FG_i$ where F is the Faraday number [38-40].

The experimental data of the electrochemical impedance $\left.\frac{\Delta E}{\Delta I}\right|_{th}(\omega)$ and the charge/potential TF, $\left.\frac{\Delta q}{\Delta E}\right|_{th}(\omega)$, were fitted using theoretical transfer functions given in Equations (A2) and (A3). In this case, two cations, *c1* and *c2* and anion, *a*, are involved in the charge compensation process.

$$\left.\frac{\Delta E}{\Delta I}\right|_{th}(\omega) = \left[j\omega d_f \left(\frac{G_{c1}}{j\omega d_f + K_{c1}} + \frac{G_{c2}}{j\omega d_f + K_{c2}} - \frac{G_a}{j\omega d_f + K_a}\right)\right]^{-1} \quad \text{(A2)}$$

$$\left.\frac{\Delta q}{\Delta E}\right|_{th}(\omega) = d_f F \left(\frac{G_{c1}}{j\omega d_f + K_{c1}} + \frac{G_{c2}}{j\omega d_f + K_{c2}} - \frac{G_a}{j\omega d_f + K_a}\right) \quad \text{(A3)}$$

The theoretical electrogravimetric transfer function, $\left.\frac{\Delta m}{\Delta E}\right|_{th}(\omega)$, can be estimated, taking into account the charged/uncharged species contribution:

$$\left.\frac{\Delta m}{\Delta E}\right|_{th}(\omega) = d_f \left(M_{c1}\frac{G_{c1}}{j\omega d_f + K_{c1}} + M_{c2}\frac{G_{c2}}{j\omega d_f + K_{c2}} + M_{c2}\frac{G_a}{j\omega d_f + K_a} + M_s\frac{G_s}{j\omega d_f + K_s}\right) \quad \text{(A4)}$$

In Equation (A4), M_{c1}, M_{c2}, M_a and M_s are the atomic weight of involved species.

From the theoretical overall electrogravimetric transfer function (Equation A4), it is possible to calculate the theoretical partial transfer functions by removing the c2 contribution, calculating $\left.\frac{\Delta m}{\Delta E}\right|_{th}^{c1as}(\omega)$; or the c1 contribution, calculating; $\left.\frac{\Delta m}{\Delta E}\right|_{th}^{c2as}(\omega)$; or the anion contribution calculating; $\left.\frac{\Delta m}{\Delta E}\right|_{th}^{c1c2s}(\omega)$, as shown in the following equations:

$$\left.\frac{\Delta m}{\Delta E}\right|_{\mathrm{th}}^{\mathrm{c1as}}(\omega) = d_f\left((M_{c1}-M_{c2})\frac{G_{c1}}{j\omega d_f+K_{c1}} + (M_a-M_{c2})\frac{G_a}{j\omega d_f+K_a} + M_s\frac{G_s}{j\omega d_f+K_s}\right) \quad \text{(A5)}$$

$$\left.\frac{\Delta m}{\Delta E}\right|_{\mathrm{th}}^{\mathrm{c2as}}(\omega) = d_f\left((M_{c2}-M_{c1})\frac{G_{c2}}{j\omega d_f+K_{c2}} + (M_a-M_{c1})\frac{G_a}{j\omega d_f+K_a} + M_s\frac{G_s}{j\omega d_f+K_s}\right) \quad \text{(A6)}$$

$$\left.\frac{\Delta m}{\Delta E}\right|_{\mathrm{th}}^{\mathrm{c1c2s}}(\omega) = d_f\left((M_{c1}-M_{c2})\frac{G_{c1}}{j\omega d_f+K_{c1}} + (M_{c2}-M_{c1})\frac{G_{c2}}{j\omega d_f+K_{c2}} + M_s\frac{G_s}{j\omega d_f+K_s}\right) \quad \text{(A7)}$$

References

[1] F. Béguin, V. Presser, A. Balducci, E. Frackowiak, Carbons and electrolytes for advanced supercapacitors, Advanced Materials 26 (2014) 2219-2251.

[2] F. Béguin, E. Raymundo-Piñero, Nanocarbons for Supercapacitors in: R. Meyers (Ed.), Encyclopedia of Sustainability Science and Technology, Springer New York2012, pp. 6769-6790.

[3] N. Ganfoud, A. Sene, M. Haefele, A. Marin-Laflèche, B. Daffos, P.-L. Taberna, M. Salanne, P. Simon, B. Rotenberg, Effect of the carbon microporous structure on the capacitance of aqueous supercapacitors, Energy Storage Materials 21 (2019) 190-195.

[4] A.G. Pandolfo, A.F. Hollenkamp, Carbon properties and their role in supercapacitors, Journal of Power Sources 157 (2006) 11-27.

[5] Y.C. Wu, J. Ye, G. Jiang, K. Ni, N. Shu, P.L. Taberna, Y. Zhu, P. Simon, Electrochemical Characterization of Single Layer Graphene/Electrolyte Interface: Effect of Solvent on the Interfacial Capacitance, Angewandte Chemie 60 (2021) 13317-13322.

[6] A. Bouzina, H. Perrot, O. Sel, C. Debiemme-Chouvy, Preventing Graphene from Restacking via Bioinspired Chemical Inserts: Toward a Superior 2D Micro-supercapacitor Electrode, ACS Applied Nano Materials 4 (2021) 4964-4973.

[7] M.P. Down, C.E. Banks, 4 - 2D materials as the basis of supercapacitor devices, in: S. Zafeiratos (Ed.), 2D Nanomaterials for Energy Applications, Elsevier2020, pp. 97-130.

[8] M.M. Islam, M.T. Alam, T. Okajima, T. Ohsaka, Electrical Double Layer Structure in Ionic Liquids: An Understanding of the Unusual Capacitance−Potential Curve at a Nonmetallic Electrode, The Journal of Physical Chemistry C 113 (2009) 3386-3389.

[9] P. Simon, Y. Gogotsi, Materials for electrochemical capacitors, Nature Materials 7 (2008) 845-854.

[10] H. Pan, J. Li, Y. Feng, Carbon Nanotubes for Supercapacitor, Nanoscale Research Letters 5 (2010) 654 - 668.

[11] P. Ratajczak, M.E. Suss, F. Kaasik, F. Béguin, Carbon electrodes for capacitive technologies, Energy Storage Materials 16 (2019) 126-145.

[12] H. Shao, Y.-C. Wu, Z. Lin, P.-L. Taberna, P. Simon, Nanoporous carbon for electrochemical capacitive energy storage, Chemical Society Reviews 49 (2020) 3005-3039.
[13] Z. Yang, J. Tian, Z. Yin, C. Cui, W. Qian, F. Wei, Carbon nanotube- and graphene-based nanomaterials and applications in high-voltage supercapacitor: A review, Carbon $V 141 (2019) 467-480.
[14] P. Simon, Y. Gogotsi, Capacitive Energy Storage in Nanostructured Carbon–Electrolyte Systems, Accounts of Chemical Research 46 (2013) 1094-1103.
[15] M.D. Levi, N. Levy, S. Sigalov, G. Salitra, D. Aurbach, J. Maier, Electrochemical Quartz Crystal Microbalance (EQCM) Studies of Ions and Solvents Insertion into Highly Porous Activated Carbons, Journal of the American Chemical Society 132 (2010) 13220-13222.
[16] M.D. Levi, G. Salitra, N. Levy, D. Aurbach, J. Maier, Application of a quartz-crystal microbalance to measure ionic fluxes in microporous carbons for energy storage, Nat Mater 8 (2009) 872-875.
[17] M.D. Levi, S. Sigalov, D. Aurbach, L. Daikhin, In Situ Electrochemical Quartz Crystal Admittance Methodology for Tracking Compositional and Mechanical Changes in Porous Carbon Electrodes, The Journal of Physical Chemistry C 117 (2013) 14876-14889.
[18] M.D. Levi, S. Sigalov, G. Salitra, R. Elazari, D. Aurbach, Assessing the Solvation Numbers of Electrolytic Ions Confined in Carbon Nanopores under Dynamic Charging Conditions, The Journal of Physical Chemistry Letters 2 (2011) 120-124.
[19] N. Shpigel, M.D. Levi, S. Sigalov, L. Daikhin, D. Aurbach, In Situ Real-Time Mechanical and Morphological Characterization of Electrodes for Electrochemical Energy Storage and Conversion by Electrochemical Quartz Crystal Microbalance with Dissipation Monitoring, Accounts of Chemical Research 51 (2018) 69-79.
[20] S. Sigalov, N. Shpigel, M.D. Levi, M. Feldberg, L. Daikhin, D. Aurbach, Electrochemical Quartz Crystal Microbalance with Dissipation Real-Time Hydrodynamic Spectroscopy of Porous Solids in Contact with Liquids, Analytical chemistry 88 (2016) 10151-10157.
[21] A. Al-zubaidi, M. Takahashi, Y. Ishii, S. Kawasaki, Switching of alternative electrochemical charging mechanism inside single-walled carbon nanotubes: a quartz crystal microbalance study, RSC Advances 11 (2021) 30253-30258.
[22] W.-Y. Tsai, P.-L. Taberna, P. Simon, Electrochemical Quartz Crystal Microbalance (EQCM) Study of Ion Dynamics in Nanoporous Carbons, Journal of the American Chemical Society 136 (2014) 8722-8728.
[23] X. Zhao, P. Xue, Y. Hou, Y. Jiao, Y. Wang, Z. Sha, In situ analysis of pore size effect of ionic solvation during the formation of double electric layers, Journal of Electroanalytical Chemistry 880 (2021) 114846.
[24] Y.-C. Wu, P.-L. Taberna, P. Simon, Tracking ionic fluxes in porous carbon electrodes from aqueous electrolyte mixture at various pH, Electrochemistry Communications 93 (2018) 119-122.
[25] J.M. Griffin, A.C. Forse, W.-Y. Tsai, P.-L. Taberna, P. Simon, C.P. Grey, In situ NMR and electrochemical quartz crystal microbalance techniques reveal the structure of the electrical double layer in supercapacitors, Nature Materials 14 (2015) 812-819.
[26] N. Shpigel, M.D. Levi, S. Sigalov, D. Aurbach, L. Daikhin, V. Presser, Novel in situ multiharmonic EQCM-D approach to characterize complex carbon pore architectures for capacitive deionization of brackish water, J Phys Condens Matter 28 (2016) 114001.
[27] V. Dargel, N. Shpigel, S. Sigalov, P. Nayak, M.D. Levi, L. Daikhin, D. Aurbach, In situ real-time gravimetric and viscoelastic probing of surface films formation on lithium batteries electrodes, Nature Communications 8 (2017) 1389.
[28] N. Shpigel, M.D. Levi, D. Aurbach, EQCM-D technique for complex mechanical characterization of energy storage electrodes: Background and practical guide, Energy Storage Materials 21 (2019) 399-413.

[29] D. Malka, R. Attias, N. Shpigel, F. Malchick, M.D. Levi, D. Aurbach, Horizons for Modern Electrochemistry Related to Energy Storage and Conversion, a Review, Israel Journal of Chemistry 61 (2021) 11-25.
[30] N. Shpigel, A. Chakraborty, F. Malchik, G. Bergman, A. Nimkar, B. Gavriel, M. Turgeman, C.N. Hong, M.R. Lukatskaya, M.D. Levi, Y. Gogotsi, D.T. Major, D. Aurbach, Can Anions Be Inserted into MXene?, Journal of the American Chemical Society 143 (2021) 12552-12559.
[31] Z. Lin, P.-L. Taberna, P. Simon, Electrochemical double layer capacitors: What is next beyond the corner?, Current Opinion in Electrochemistry 6 (2017) 115-119.
[32] F. Escobar-Teran, A. Arnau, J.V. Garcia, Y. Jiménez, H. Perrot, O. Sel, Gravimetric and dynamic deconvolution of global EQCM response of carbon nanotube based electrodes by Ac-electrogravimetry, Electrochemistry Communications 70 (2016) 73-77.
[33] F. Escobar-Teran, H. Perrot, O. Sel, Ion Dynamics at the Single Wall Carbon Nanotube Based Composite Electrode/Electrolyte Interface: Influence of the Cation Size and Electrolyte pH, The Journal of Physical Chemistry C 123 (2019) 4262-4273.
[34] H. Goubaa, F. Escobar-Teran, I. Ressam, W. Gao, A. El Kadib, I.T. Lucas, M. Raihane, M. Lahcini, H. Perrot, O. Sel, Dynamic Resolution of Ion Transfer in Electrochemically Reduced Graphene Oxides Revealed by Electrogravimetric Impedance, The Journal of Physical Chemistry C 121 (2017) 9370-9380.
[35] W. Gao, C. Debiemme-Chouvy, M. Lahcini, H. Perrot, O. Sel, Tuning Charge Storage Properties of Supercapacitive Electrodes Evidenced by In Situ Gravimetric and Viscoelastic Explorations, Analytical chemistry 91 (2019) 2885-2893.
[36] C.R. Arias, C. Debiemme-Chouvy, C. Gabrielli, C. Laberty-Robert, A. Pailleret, H. Perrot, O. Sel, New Insights into Pseudocapacitive Charge-Storage Mechanisms in Li-Birnessite Type MnO2Monitored by Fast Quartz Crystal Microbalance Methods, The Journal of Physical Chemistry C 118 (2014) 26551-26559.
[37] E.M. Halim, M. Elbasri, H. Perrot, O. Sel, K. Lafdi, M. El Rhazi, Synthesis of carbon nanofibers/poly(para-phenylenediamine)/nickel particles nanocomposite for enhanced methanol electrooxidation, International Journal of Hydrogen Energy 44 (2019) 24534-24545.
[38] P. Lemaire, O. Sel, D. Alves Dalla Corte, A. Iadecola, H. Perrot, J.-M. Tarascon, Elucidating the Origin of the Electrochemical Capacity in a Proton-Based Battery HxIrO4 via Advanced Electrogravimetry, ACS Applied Materials & Interfaces 12 (2020) 4510-4519.
[39] F. Escobar-Teran, H. Perrot, O. Sel, Charge storage properties of single wall carbon nanotubes/Prussian blue nanocube composites studied by multi-scale coupled electrogravimetric methods, Electrochimica Acta 271 (2018) 297-304.
[40] C. Gabrielli, J.J. García-Jareño, M. Keddam, H. Perrot, F. Vicente, Ac-Electrogravimetry Study of Electroactive Thin Films. I. Application to Prussian Blue, The Journal of Physical Chemistry B 106 (2002) 3182-3191.
[41] C. Gabrielli, J.J. Garcia-Jareño, M. Keddam, H. Perrot, F. Vicente, Ac-Electrogravimetry Study of Electroactive Thin Films. II. Application to Polypyrrole, The Journal of Physical Chemistry B 106 (2002) 3192-3201.
[42] G. Mercier, C. Hérold, J.-F. Marêché, S. Cahen, J. Gleize, J. Ghanbaja, G. Lamura, C. Bellouard, B. Vigolo, Selective removal of metal impurities from single walled carbon nanotube samples, New Journal of Chemistry 37 (2013) 790-795.
[43] M.D. Levi, S. Sigalov, G. Salitra, D. Aurbach, J. Maier, The effect of specific adsorption of cations and their size on the charge-compensation mechanism in carbon micropores: the role of anion desorption, Chemphyschem : a European journal of chemical physics and physical chemistry 12 (2011) 854-862.

[44] S. Bruckenstein, A.R. Hillman, Consequences of thermodynamic restraints on solvent and ion transfer during redox switching of electroactive polymers, The Journal of Physical Chemistry 92 (1988) 4837-4839.
[45] H.M. French, M.J. Henderson, A.R. Hillman, E. Vieil, Temporal resolution of ion and solvent transfers at nickel hydroxide films exposed to LiOH, Solid State Ionics 150 (2002) 27-37.
[46] H.M. French, M.J. Henderson, A.R. Hillman, E. Vieil, Ion and solvent transfer discrimination at a nickel hydroxide film exposed to LiOH by combined electrochemical quartz crystal microbalance (EQCM) and probe beam deflection (PBD) techniques, Journal of Electroanalytical Chemistry 500 (2001) 192-207.
[47] M. Gonsalves, A. Robert Hillman, Effect of time scale on redox-driven ion and solvent transfers at nickel hydroxide films in aqueous lithium hydroxide solutions, Journal of Electroanalytical Chemistry 454 (1998) 183-202.
[48] F. Razzaghi, C. Debiemme-Chouvy, F. Pillier, H. Perrot, O. Sel, Ion intercalation dynamics of electrosynthesized mesoporous WO3 thin films studied by multi-scale coupled electrogravimetric methods, Physical Chemistry Chemical Physics 17 (2015) 14773-14787.